Taylor & Francis
Taylor & Francis Group

Modelling and experimental validation of the displacement of a check valve in a hydraulic piston pump

Anthony L. Knutson [ID] and James D. Van de Ven

Department of Mechanical Engineering, University of Minnesota, Minneapolis, MN, USA

ABSTRACT

A variety of methods have previously been applied to modelling hydraulic check valves. While the theoretical framework has been established, robust experimental validation of check valve models is lacking. When present, validation methods typically rely on measurements of pressure differential or flow rates, from which check valve dynamics are inferred. In this paper, a lumped parameter model is constructed for a disc style check valve used to control the inlet and outlet flow of a piston pump. Pressure, spring, contact, stiction, and flow forces are investigated to determine which have a significant effect on the check valve dynamics. An experimental pump circuit is constructed and an acrylic sight glass is installed on the check valve manifolds. A method of directly measuring the check valve position during operation using a Laser Triangulation Sensor (LTS) is developed by applying Snell's law to the air-acrylic and acrylic-oil interfaces and calculating laser refraction to obtain a relationship between valve position and LTS voltage output. Modelled valve position and flow rates are compared to experimental data for three sets of operating conditions – baseline, high speed, and high pressure. In all three cases, modelled inlet and delivery valve displacement closely agree with experimental measurements. Error between predicted and measured flow rates is less than 3% for all cases.

1. Introduction

A check valve is a passive device that allows unidirectional flow. Often, check valves are used in quasi-static situations, such as component bypass and cylinder locking, where the dynamic behaviour of the check valve is not critical. However, some applications require fast valve response to pressure changes with minimal backflow, such as pumps, digital hydraulics, and servo hydraulic circuits. While the behaviour of a valve could be predicted through a multi-dimensional, multi-domain computational fluid dynamics simulation, this approach is computationally expensive and not appropriate for iterative design and optimisation. In this paper, a dynamic check valve model, developed through a coupled analytical and experimental approach, will be presented and validated experimentally.

Researchers have modelled hydraulic pumps containing check valves and performed experiments to compare predicted and measured results. Johnston (1991) achieved good correlation between simulated and measured valve position, flow rate, and pressure. However, the method used to measure valve position is not described by Johnston. Additionally, the poppet valves used by Johnston had masses of 270 and 430 g – over 100 times greater than commercially available disc valve investigated in this paper – raising question to the

validity of the model in high frequency applications. Edge *et al.* (1984) modelled an eight-cylinder radial diaphragm pump with check valves comparing simulated and experimental flow rate and cylinder pressure. Lee *et al.* (2015) modelled check valves in a three cylinder reciprocating pump using a correction factor for the cross-sectional area of the valve and bulk modulus correlation coefficients as tuning parameters to match simulated and measured cylinder pressure. Due to the dynamic behaviour of a check valve opening and closing, measuring only the pressure and flow rate does not fully describe the motion of the check valve. A superior way of validating a check valve model is directly measuring the motion of the moving element.

This work proposes a novel method of experimentally validating check valve models by optically measuring valve position at high speeds using a Laser Triangulation Sensor (LTS). To accomplish this, a check valve model is presented and integrated into a single cylinder pump model similar to Johnston (1991) but without the simplifying assumptions of a constant fluid bulk modulus and constant valve discharge coefficients. While these two assumptions are common in literature, they have a significant limiting effect on the performance of hydraulic pump models. These simplifications are eliminated by incorporating a pressure dependent bulk modulus

CONTACT James D. Van de Ven [envelope] vandeven@umn.edu

model proposed by Cho *et al.* (2002) and an experimentally determined discharge coefficient correlation. The check valve model is presented in two parts. First, the individual forces acting on the moving element are considered to develop a model of valve motion. Second, a model of flow rate through the valve is developed using a semi-empirical approach. Next, an experimental setup capable of validating the check valve model is described. Finally, experimental results are presented that validate the proposed check valve model followed by a discussion of the results.

2. Pump model

A single cylinder pump is modelled using a lumped parameter approach (Figure 1). In three discrete regions – the tank, pump cylinder, and accumulator – the pressure is assumed to be spatially uniform. The corresponding locations where the fluid pressure is assumed to change instantaneously are the inlet and delivery check valves and the variable orifice (VO).

Six differential equations are numerically solved to calculate cylinder and load pressure and inlet and delivery valve position and velocity. The cylinder pressure, P_{cyl}, is calculated from the definition of the effective bulk modulus, β_{eff}, as:

$$\frac{dP_{cyl}}{dt} = \frac{\beta_{eff}\left(P_{cyl}\right)}{V_{cyl}}\left(Q_{inlet} - Q_{delivery} - \frac{dV_{cyl}}{dt}\right) \quad (1)$$

where V_{cyl} is the instantaneous cylinder volume and Q_{inlet} and $Q_{delivery}$ are the volumetric flow rate through the inlet and delivery check valve respectively. For the inlet valve, flow into the cylinder is defined as positive whereas flow out of the cylinder is defined as positive for the delivery valve. Leakage is assumed to be negligible. The effective bulk modulus of the hydraulic oil is modelled using the approach developed by Cho *et al.* (2002).

$$\beta_{eff}\left(P_{cyl}\right) = \beta \left[\frac{\left(\frac{P_{cyl}}{P_o}\right)^{\frac{1}{\gamma}} e^{\frac{\left(P_o - P_{cyl}\right)}{\beta}} + R}{\frac{R}{\gamma}\frac{\beta}{P_{cyl}} + \left(\frac{P_{cyl}}{P_o}\right)^{\frac{1}{\gamma}} e^{\frac{\left(P_o - P_{cyl}\right)}{\beta}}} \right] \quad (2)$$

where β is the bulk modulus of air free oil, P_o is atmospheric pressure, γ is the ratio of specific heats for air, and R is the percent air content by volume at atmospheric pressure.

The instantaneous cylinder volume is the sum of the volume at top dead centre, V_{tdc}, and the volume swept by the piston given by:

$$V_{cyl} = V_{tdc} + A_{piston}\left[r(1 - \cos\theta) + l - \sqrt{l^2 - r^2 \sin^2\theta}\right] \quad (3)$$

where A_{piston} is the area of the piston, r and l are the crank radius and connecting rod length respectively, and θ is
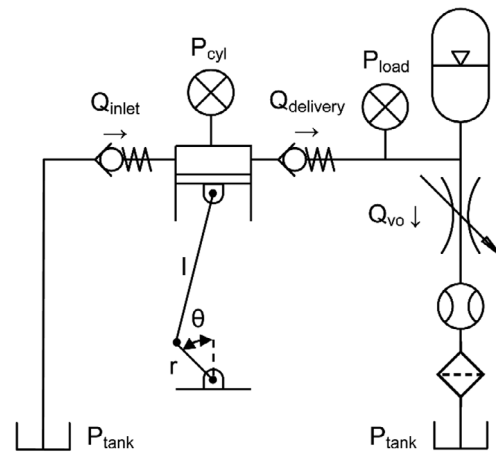
Figure 1. Pump circuit schematic.

the crank angle from top dead center. The time rate of change of the cylinder volume is then calculated from the pump speed, ω, as:

$$\frac{dV_{cyl}}{dt} = A_{piston}\omega r \sin\theta \left[1 + \frac{r\cos\theta}{\sqrt{l^2 - r^2 \sin^2\theta}}\right] \quad (4)$$

A gas loaded accumulator and a VO are placed downstream of the delivery valve. The accumulator is charged with nitrogen, which is approximated as an ideal gas undergoing isentropic compression and expansion. The load pressure, P_{load}, is then given as a function of the charge pressure, P_{charge}, charge volume, V_{charge}, instantaneous accumulator gas volume, V_{acc}, and ratio of specific heats for nitrogen by:

$$P_{load} = P_{charge}\left(\frac{V_{charge}}{V_{acc}}\right)^{\gamma} \quad (5)$$

The accumulator gas volume is calculated by assuming the hydraulic fluid compressibility is negligible compared to that of the nitrogen gas and applying mass conservation to the load line to obtain:

$$\frac{dV_{acc}}{dt} = Q_{vo} - Q_{delivery} \quad (6)$$

where Q_{vo} is the volumetric flow rate through the VO.

Downstream of the VO are a gear flow metre and 10 micron filter in series. Associated with each of these components is a flow rate dependent pressure drop. The pressure drop relationship is assumed to be of the form

$$\Delta P_{comp} = C_{comp}Q_{comp}^2 \quad (7)$$

where ΔP_{comp}, C_{comp}, and Q_{comp}, are the component pressure drop, pressure drop coefficient, and volumetric flow rate respectively. The gear flow meter and filter manufacturers provide pressure drop charts, from which pressure drop coefficients were estimated. Applying the steady orifice equation, the pressure drop across the VO, ΔP_{vo}, is:

$$\Delta P_{\text{vo}} = \frac{\rho Q_{\text{vo}}^2}{2\left(C_{\text{d}}A_{\text{o}}\right)^2_{\text{vo}}} \qquad (8)$$

where $\left(C_{\text{d}}A_{\text{o}}\right)_{\text{vo}}$ is the product of the discharge coefficient and effective orifice area of the VO and ρ is the hydraulic oil density. The total pressure drop between the load and tank is then given by:

$$P_{\text{load}} - P_{\text{tank}} = \Delta P_{\text{vo}} + \Delta P_{\text{meter}} + \Delta P_{\text{filter}} \qquad (9)$$

where P_{tank} is the tank pressure. Solving for Q_{vo} yields:

$$Q_{\text{vo}} = \sqrt{\frac{P_{\text{load}} - P_{\text{tank}}}{\frac{\rho}{2\left(C_{\text{d}}A_{\text{o}}\right)^2_{\text{vo}}} + C_{\text{meter}} + C_{\text{filter}}}} \qquad (10)$$

3. Check valve model

The check valve in this study is a disc style, although the process for modelling a poppet or ball style valve is similar. One advantage of a disc valve is the low mass of the moving element, which allows for faster response. A diagram of the disc valve is shown in Figure 2.

3.1. Valve motion

The valve motion governing equations are derived by applying Newton's second law to the valve disc and replacing a single, second order differential equation with two, first order differential equations as follows:

$$\frac{\text{d}x}{\text{d}t} = v \qquad (11)$$

$$\frac{\text{d}v}{\text{d}t} = \frac{F}{m} \qquad (12)$$

where x and v are the valve position and velocity respectively, F is the net force acting on the valve, and m is the valve mass.

The forces acting on the valve disc are the pressure force, spring force, contact force, stiction force, steady flow force, and transient flow force. The pressure force is calculated as the pressure differential across the check valve, ΔP_{valve}, multiplied by the disc area, A_{valve}.

$$F_{\text{pressure}} = \Delta P_{\text{valve}} A_{\text{valve}} \qquad (13)$$

The spring force is expressed as:

$$F_{\text{spring}} = -k_{\text{spring}}\left(x + x_{\text{preload}}\right) \qquad (14)$$

where k_{spring} is the spring stiffness and x_{preload} is valve spring preload. The contact force of the seat and stop is the sum of the elastic and dissipative reaction forces.

$$F_{\text{contact}} = \begin{cases} -k_{\text{seat}}x - c_{\text{seat}}v, & \text{if } x < 0 \\ 0, \text{if } 0 \le x \le x_{\text{stop}} \\ -k_{\text{stop}}\left(x - x_{\text{stop}}\right) - c_{\text{stop}}v, & \text{if } x < x_{\text{stop}} \end{cases} \qquad (15)$$
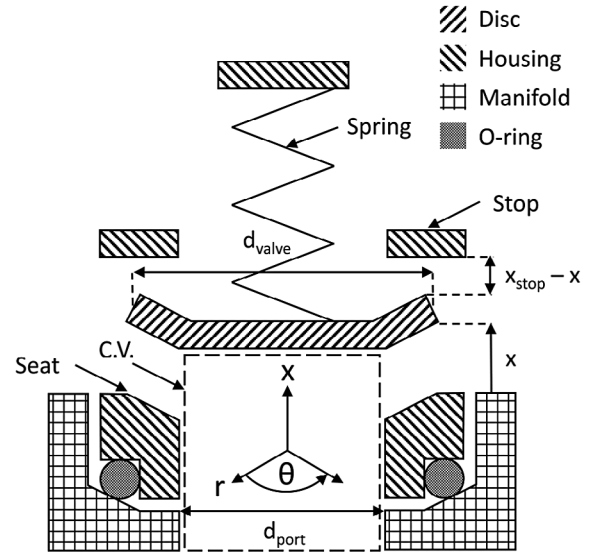
Figure 2. Disc style check valve diagram.

where k_{seat} and k_{stop} are the spring stiffness of the valve seat and stop respectively, c_{seat} and c_{stop} are the damping coefficients of the valve seat and stop respectively, and x_{stop} is the maximum valve opening. Note that the seat spring stiffness and damping coefficient can depend not only on the material properties and geometry of the disc and housing, but also the O-ring if there is space between the housing and manifold, as shown in Figure 2. Values of k and c were estimated by adjusting each individually until the modelled seat and stop deflection and valve bounce most closely followed experimental measurements.

To satisfy continuity when the valve is opening or closing, fluid must fill or evacuate the gap between the disc and the seat. When the gap height is very small, the flow can be modelled as Couette flow. To drive this flow, a pressure gradient develops which opposes the valve motion, resulting in a stiction force. For a flat disc that remains parallel to a flat seat, the stiction force can is calculated (Hamrock *et al.* 2004) as:

$$F_{\text{stiction}} = C\frac{v}{(x + h)^3} \qquad (16)$$

where C is the stiction coefficient and h is the minimum oil gap thickness. The stiction coefficient is given by:

$$C = \frac{3\pi\mu}{32}\left(d_{\text{port}}^4 - d_{\text{valve}}^4\right) \\ \left[1 - \frac{d_{\text{valve}}^2 - d_{\text{port}}^2}{\left(d_{\text{valve}}^2 + d_{\text{port}}^2\right)\left(\ln d_{\text{valve}} - \ln d_{\text{port}}\right)}\right] \qquad (17)$$

where μ is the dynamic viscosity of the hydraulic oil.

Steady and transient flow forces acting on a spool valve were derived by Merritt (1967). Similarly, flow forces acting on a check valve are derived by applying Reynolds transport theorem to a control volume of fluid

in the vicinity of the valve as shown in Figure 2. In the following analysis, only the flow forces along the *x*-axis are considered. The steady flow force, which represents the change in momentum of the fluid entering and exiting the control volume, is expressed as:

$$F_{\text{steady}} = \rho \frac{Q^2}{A_{\text{port}}} \qquad (18)$$

The transient flow force represents the force associated with the change of momentum of fluid within the control volume as it accelerates and is given by:

$$F_{\text{transient}} = -\rho L \frac{dQ}{dt} \qquad (19)$$

where *L* is the damping length, estimated to be equal to the port diameter. The net force acting on the valve is then calculated as:

$$F = F_{\text{pressure}} + F_{\text{spring}} + F_{\text{contact}} + F_{\text{stiction}} + F_{\text{transient}} \quad (20)$$

The magnitude of stiction and flow forces were found to be negligible as described in Section 5. Based on these findings, stiction and flow forces were not included in the model results presented. Note that for some geometries and operating conditions stiction and/or flow forces may be significant so it should be determined for each individual case if either has a significant effect on valve motion.

3.2. Valve flow rate

The flow rate through the check valve is found by modelling it as an orifice. For steady flow of an incompressible fluid, the volumetric flow rate through an orifice, Q_{o}, is related to the pressure differential across the orifice, ΔP, by:

$$Q_{\text{o}} = C_{\text{d}} A_0 \sqrt{\frac{2|\Delta P|}{\rho}} \text{sign}(\Delta P) \qquad (21)$$

where C_{d} is the discharge coefficient and A_{o} is the orifice area. Although Equation (21) is derived for steady flow, it is commonly assumed to approximate transient flow rates. The orifice area of the disc valve is calculated as:

$$A_{\text{o}}(x) = \max(\pi d_{\text{port}} x, 0) \qquad (22)$$

where d_{port} is the valve port diameter. The orifice area may also be defined as normal to the seat surface although the difference between the two definitions was calculated and found to be negligible so the simpler expression was used. Since the discharge coefficient is a function of the Reynolds number and therefore flow rate, an iterative process is required to calculate the flow rate.

The total flow rate into or out of the piston cylinder is the sum of the orifice flow rate through the valve and the
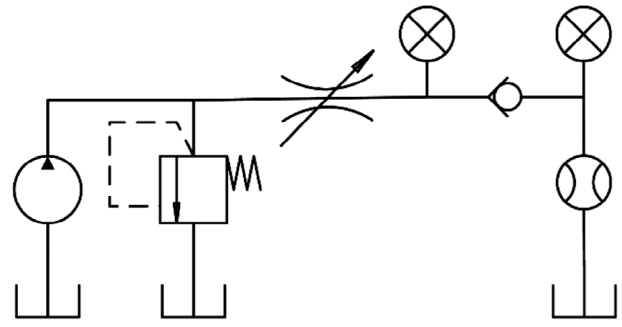
Figure 3. Discharge coefficient experimental setup.

rate of fluid displacement caused by the disc displacement. The inlet valve flow rate is calculated as:

$$Q_{\text{inlet}} = C_{\text{d}} A_{\text{o}} \sqrt{\frac{2|P_{\text{tank}} - P_{\text{cyl}}|}{\rho}} \times \text{sign}\left(P_{\text{tank}} - P_{\text{cyl}}\right) + A_{\text{valve}} v_{\text{inlet}} \qquad (23)$$

Similarly, the flow rate through the delivery valve is given by:

$$Q_{\text{delivery}} = C_{\text{d}} A_{\text{o}} \sqrt{\frac{2|P_{\text{cyl}} - P_{\text{load}}|}{\rho}} \times \text{sign}\left(P_{\text{cyl}} - P_{\text{load}}\right) + A_{\text{valve}} v_{\text{delivery}} \qquad (24)$$

3.3. Valve discharge coefficient measurement

To experimentally determine the discharge coefficient of the check valve, a hydraulic power unit was placed in series with a VO, which allows the flow rate through the check valve to be prescribed. Two pressure transducers measure the pressure differential across the check valve while a gear flow metre measures the flowrate through it. The check valve disc displacement was set with a shim that controls the maximum disc opening, allowing calculation of the orifice area. Figure 3 shows the experimental setup.

In this paper, the discharge coefficient is defined as:

$$C_{\text{d}} = \frac{Q_{\text{o}}}{A_{\text{o}} \sqrt{\frac{2\Delta P}{\rho}}} \qquad (25)$$

The Reynolds number, *Re*, is calculated using the hydraulic diameter of the valve orifice as:

$$\text{Re} = \frac{4\rho Q_o}{\mu P} \qquad (26)$$

where the perimeter, *P*, is the twice the circumference of the valve port. Wu *et al.* (2002) proposed an empirical discharge coefficient model of the form:

$$C_{\text{d}} = C_{d\infty} + A e^{-B\sqrt{\text{Re}}} - \left(C_{d\infty} + A\right) e^{-C\sqrt{\text{Re}}} \quad (27)$$
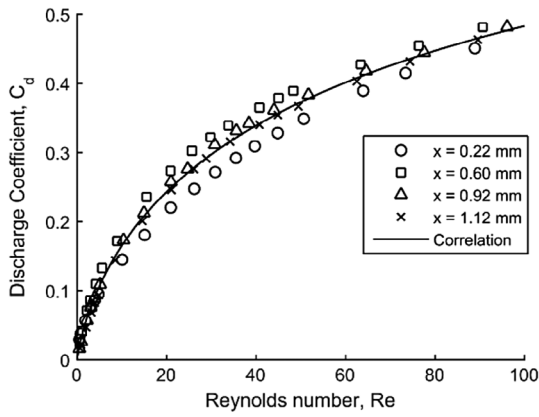
Figure 4. Discharge coefficient correlation.
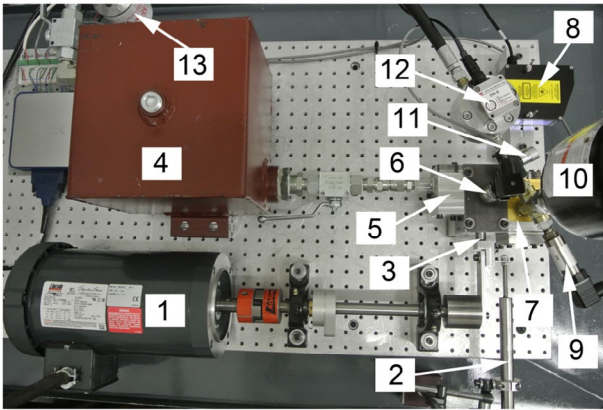
Figure 5. Instrumented experimental setup consisting of a (1) Motor, (2) Piston, (3) LVDT, (4) Tank, (5) Inlet check valve, (6) Cylinder pressure transducer, (7) Delivery check valve, (8) LTS, (9) Load pressure transducer, (10) Accumulator, (11) Adjustable orifice valve, (12) Gear flow metre and (13) Filter.

A nonlinear least squares fit was then applied to experimental measurements to obtain the following correlation:

$$C_d = 0.7864 - 0.8738 e^{-0.1058\sqrt{Re}} + 0.0874 e^{-0.9505\sqrt{Re}}$$

(28)

The experimental results and Equation (28) are shown in Figure 4, where x in the legend is the valve displacement.

The results show that while the discharge coefficient is a strong function of the Reynolds number, there is no clear dependence on valve opening. Note that Equation (28) is only valid across the range of Reynolds numbers used to obtain the correlation. The maximum Reynolds number reached during pumping experiments was approximately 68.

4. Experimental approach

To validate the check valve model, experiments are performed using a single cylinder crank-slider piston pump shown in Figure 5. The pump crankshaft is driven by an electric motor controlled by a variable frequency drive.
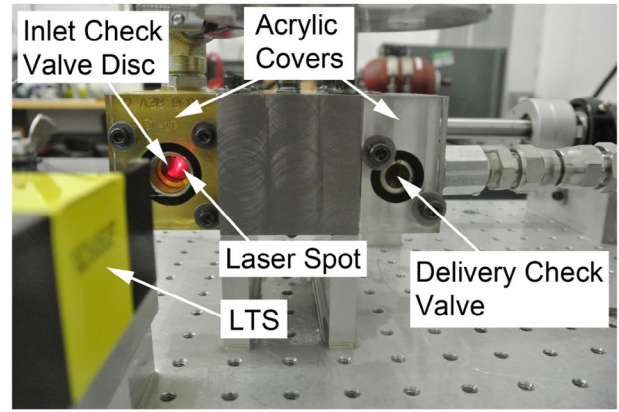
Figure 6. Valve position measurement with a LTS.

Piston position is measured using a linear variable differential transformer (LVDT) displacement transducer attached directly to the piston. Both the inlet and delivery valve manifolds have acrylic covers to allow an LTS to measure the position of the valve discs as shown in Figure 6.

Cylinder and load pressure are measured with Silicon-on-Sapphire pressure transducers with a response time of 0.2 ms. A positive displacement gear flow metre measures the average volumetric flow rate downstream of the VO. All measurements were taken at a sampling frequency of 10 kHz. The circuit parameters used in the model and experimental setup are given in Table 1.

4.1. Refractive index measurement

In order to measure the positon of the check valve, the refractive index of hydraulic oil and acrylic must first be determined. Figure 7 shows the experimental setup used to measure the index of refraction. The laser angle, θ_a, is calculated from the experiment geometry as:

$$\theta_a = \tan^{-1}\left(\frac{C_2}{C_1 + L_s}\right)$$

(29)

where L_s is the standoff length and C_1 and C_2 are constants determined by the LTS geometry. Combining Snell's law and measurements of the experimental setup geometry, the refractive index of the material is calculated as:

$$n_m = n_a \sin\theta_a \sqrt{\left[\frac{t_m}{C_2 - (C_1 + t_a)\tan\theta_a}\right]^2 + 1}$$

(30)

Water and 70% isopropyl alcohol were used to estimate the measurement error. Table 2 summarises the measurements used to experimentally determine the refractive indices. Note that although the refractive index of acrylic is readily available in literature, it is a function of the manufacturing technique and thus was determined experimentally.

Table 1. Pump experimental parameters.

Parameter	Symbol	Units	Value
Valve seat damping coefficient – inlet	c_{seat}	N*s/m	1×10^4
Valve seat damping coefficient – delivery	c_{seat}	N*s/m	1×10^3
Valve stop damping coefficient	c_{stop}	N*s/m	1×10^4
Stiction coefficient	C	N*m²s	-3.16×10^{-11}
Product of VO discharge coefficient and area	$(C_d A_o)_{vo}$	m²	$1.83 \times 10^{-7} – 2.77 \times 10^{-7}$
Filter pressure drop coefficient	C_{filter}	Pa*s²/m⁶	1.10×10^{12}
Flow meter pressure drop coefficient	C_{meter}	Pa*s²/m⁶	1.02×10^{13}
Piston diameter	d_{piston}	mm	15.88
Valve port diameter	d_{port}	mm	10.48
Valve face diameter	d_{valve}	mm	15.00
Valve spring stiffness	k	N/m	213
Valve seat spring stiffness – inlet	k_{seat}	N/m	1×10^9
Valve seat spring stiffness – delivery	k_{seat}	N/m	1.5×10^6
Valve stop spring stiffness	k_{stop}	N/m	1×10^9
Connecting rod length	l	mm	86
Damping length	L	mm	10.48
Disc mass	m	g	2.5
Atmospheric pressure	P_o	kPa	101.325
Accumulator charge pressure	P_{charge}	MPa	2.71–3.80
Tank pressure	P_{tank}	kPa	101.325
Crank radius	r	mm	5.6
Air fraction by volume	R	fraction	0.01
Pump displacement	V	cc/rev	2.22
Cylinder volume at top dead center	V_{tdc}	m³	2.17×10^{-5}
Accumulator volume	V_{charge}	litre	0.946
Valve spring preload	x_{pre}	mm	6.2
Maximum valve opening – inlet	x_{stop}	mm	1.19
Maximum valve opening – delivery	x_{stop}	mm	1.01
Bulk modulus of air free oil	β	GPa	1.84
Ratio of specific heats for air/nitrogen	γ	ratio	1.4
Hydraulic oil dynamic viscosity	μ	Pa*s	0.0683
Hydraulic oil density	ρ	kg/m³	876
Pump speed	ω	rpm	591–744

In this paper, uncertainty in a quantity f which is a function of variables $x_1, \ldots, x_n$ is calculated as follows:

$$\Delta f(x_1, \ldots, x_n) = \quad (31)$$

$$\sum_{i=1}^{n} \left| f(x_1, \ldots, x_i + \Delta 0 x_i, \ldots, x_n) - f(x_1, \ldots, x_n) \right|$$

The results of the refractive index experiments are reported in Table 3. The percent error for water was larger than the estimated uncertainty. This may be due to impurities as tap water was used rather than distilled.

4.2. LTS measurement

To experimentally validate the model, the position of the check valve disc was optically measured with an LTS. A method for measuring liquid film thickness through quartz using a LTS, developed by Peterson and Peterson (2006), was modified for measuring the check valve disc position in hydraulic oil through acrylic (PMMA). The sensor output voltage, ΔV, is converted to the apparent change in position, x_{app}, using an apparent scale factor, C_{app}, which is specified by the manufacturer for measurements taken through air. Refraction of the laser light at the air-acrylic and acrylic oil interfaces changes the scale factor and introduces nonlinearity (Yudell and Van de Ven 2015). The actual scale factor, C_{act}, can be estimated experimentally by measuring the change in output voltage given a known actual change in position, x_{act}. While this method is simple, its use is limited to the
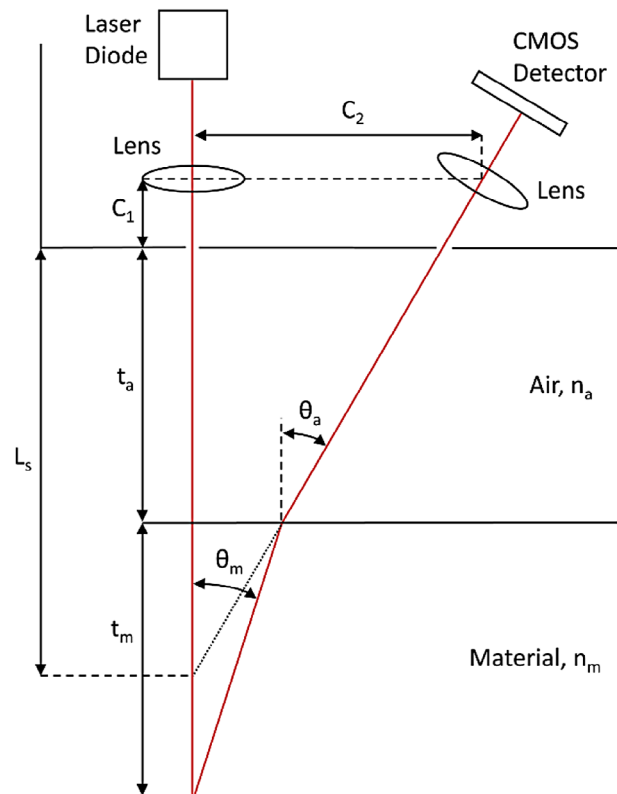
Figure 7. Experimental setup to measure index of refraction.

experimental setup. To avoid this limitation, a method to analytically calculate the actual scale factor was developed. Figure 8 shows a LTS measuring a change in position through an acrylic sight glass and hydraulic oil.

Table 2. Refractive index experiment measurements.

Symbol	Units	Value
C_1	mm	8.35 ± 0.10
C_2	mm	44.06 ± 0.10
n_a	ratio	1.000 ± 0.000
$t_{a, water}$	mm	96.12 ± 0.10
t_{water}	mm	32.23 ± 0.20
$t_{a, alcohol}$	mm	97.39 ± 0.10
$t_{alcohol}$	mm	32.23 ± 0.20
$t_{a, oil}$	mm	98.82 ± 0.10
t_{oil}	mm	32.23 ± 0.20
$t_{a, acrylic}$	mm	112.21 ± 0.10
$t_{acrylic}$	mm	12.13 ± 0.05

The variables $C_1, C_2, L_s, t_a, t_p, n_a, n_p$, and n_o, defined in Table 4, were measured and the actual change in position was chosen as an input, leaving nine unknown variables – six laser angles, θ, oil gap thickness, t_o, apparent change in position, and the sensor output voltage. Therefore nine equations are required to solve for the output voltage given the actual change in position. Snell's law provides four equations:

$$\frac{n_a}{n_p} = \frac{\sin \theta_{p1}}{\sin \theta_{a1}} \tag{32}$$

$$\frac{n_p}{n_o} = \frac{\sin \theta_{o1}}{\sin \theta_{p1}} \tag{33}$$

$$\frac{n_a}{n_p} = \frac{\sin \theta_{p2}}{\sin \theta_{a2}} \tag{34}$$

$$\frac{n_p}{n_o} = \frac{\sin \theta_{o2}}{\sin \theta_{p2}} \tag{35}$$

An additional four equations can be derived from the geometry of the experimental setup:

$$\tan \theta_{a1} = \frac{C_2}{C_1 + L_s} \tag{36}$$

$$\left(C_1 + t_a\right) \tan \theta_{a1} + t_p \tan \theta_{p1} + t_o \tan \theta_{o1} = C_2 \tag{37}$$

$$\left(C_1 + t_a\right) \tan \theta_{a2} + t_p \tan \theta_{p2} + (t_o + x_{act}) \tan \theta_{o2} = C_2 \tag{38}$$

$$x_{app} = C_2 \left(\frac{1}{\tan \theta_{a2}} - \frac{1}{\tan \theta_{a1}} \right) \tag{39}$$

Lastly, by definition the apparent scale factor is related to the apparent change in position by:

$$C_{app} = \frac{x_{app}}{\Delta V} \tag{40}$$

Rather than seek an analytical solution for the actual change in position as a function of the sensor output voltage, Equations (32) through (40) are solved numerically for 11 discrete values of the actual change in position between 0 and 1.2 mm. The resulting relationship is highly linear so the actual scale factor was calculated for the inlet and delivery valves as the slope of a least squares linear fit as shown in Figure 9.

The actual scale factors calculated for inlet and delivery valves were 3.751 and 3.740 mm/V respectively. From the actual scale factors, the position of the disc can be calculated from LTS voltage data as:

$$x_{act} = C_{act} \Delta V \tag{41}$$

The input parameters that define the LTS experimental measurements are given in Table 4.

From Equation (31) the uncertainty in the actual scale factor for the inlet and delivery valve manifold are ± 1.120 and $\pm 1.111\%$ respectively. Since the uncertainty in the voltage measurement is significantly smaller than the uncertainty in the actual scale factors, the uncertainty of the position measurement as calculated from Equation (41) is approximately equal to that of the actual scale factors. The difference in actual scale factor between the inlet and delivery valve manifold is due to the difference in thickness of the air gap, sight glass, and oil as shown in Table 4.

4.3. Experimental methods

Three experimental conditions are used to validate the valve model, as summarised in Table 5. Note that the load pressure varies throughout a revolution as a result of accumulator charging and discharging as well as between experiments due to the coarse control of the VO.

Experiments were performed by first setting the motor speed. Next, the load pressure was set by adjusting the VO and allowing the pump to run until the load pressure reached cyclic steady state. Data was collected for a period of five seconds. During post processing, the timing of top dead centre, which was used to align model and experimental results, was determined from LVDT piston position data. Several experiments were performed at each condition and the results shown in the following section are typical results.

Table 3. Refractive index experiment results (Chu and Thompson 1962, Budwig 1994).

Material	Water	Isopropanol, 70%	Hydraulic oil	Acrylic
n, Measured	$1.318 \pm 0.9932\%$	$1.387 \pm 1.024\%$	$1.476 \pm 1.062\%$	$1.509 \pm 1.668\%$
n, Literature	1.3312	1.3742	NA	1.489
% Error	0.997	0.927	NA	1.334
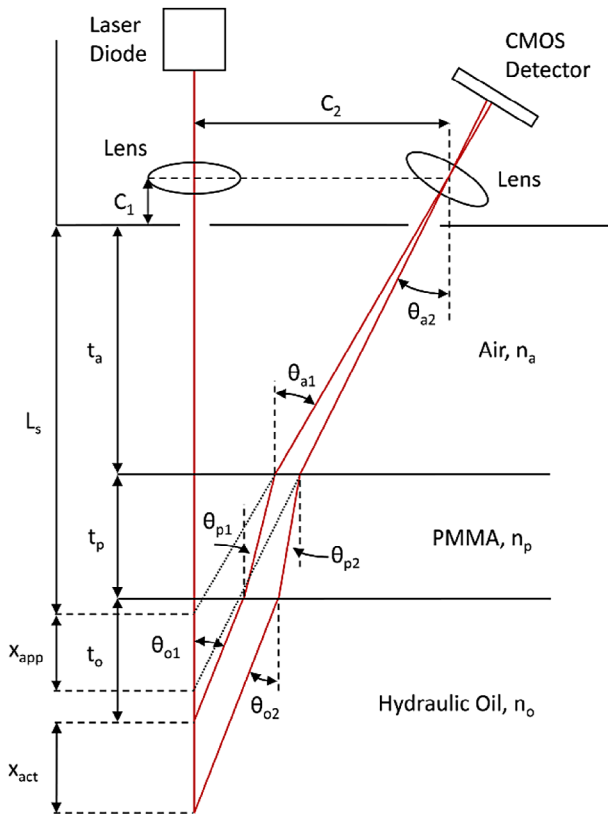
Figure 8. LTS position measurement.

Table 5. Experimental conditions.

Condition	Load pressure (MPa)	Pump speed (rpm)
Baseline	2.73–2.82	593–594
High pressure	3.63–3.80	591–592
High speed	2.71–2.83	743–744
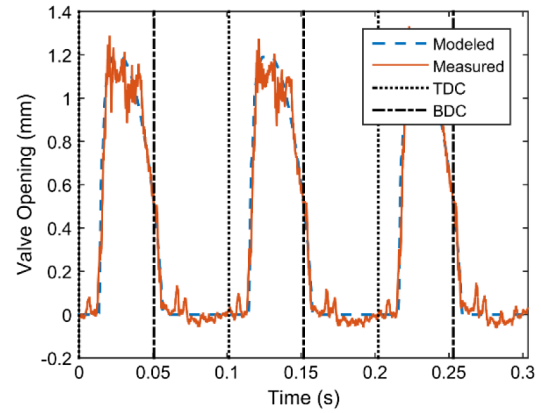
Figure 10. Inlet valve position, baseline.

Table 4. LTS position measurement input parameters.

Parameter	Symbol	Units	Value
Apparent analog out scale factor	C_{app}	mm/V	2.50 ± 0.00
LTS geometric constant	C_1	mm	8.35 ± 0.10
LTS geometric constant	C_2	mm	44.06 ± 0.10
Standoff length	L_s	mm	120.00 ± 0.00
Refractive index of air	n_a	ratio	1.000 ± 0.000
Refractive index of hydraulic oil	n_o	ratio	1.476 ± 0.016
Refractive index of PMMA	n_p	ratio	1.509 ± 0.025
Thickness of air gap – inlet valve	t_a	mm	90.67 ± 0.10
Thickness of PMMA sight glass – inlet valve	t_p	mm	12.14 ± 0.05
Thickness of air gap – delivery valve	t_a	mm	84.10 ± 0.10
Thickness of PMMA sight glass – delivery valve	t_p	mm	11.84 ± 0.05
Actual change in position	x_{act}	mm	$(0.00–1.20) \pm 0.00$

5. Results and discussion

To compare experimental and simulation results, time is defined as zero at top dead centre of the piston. Experimental inlet and delivery valve disc position data for the baseline case, the high pressure case, and the high speed case are compared to model results in Figures 10–13. While six experiments were performed, the inlet valve dynamics did not change significantly between baseline and high pressure experiments. Similarly, the delivery valve dynamics did not change significantly between baseline and high speed experiments. As such, plots from these experiments are not included.

A distinctive feature of the experimental disc position measurements is oscillations occurring when the valve is open. High speed video taken of the valves during pumping shows the disc wobbling after opening. At the instants shown, the disc is untilted in Figure 14(a) and tilted in Figure 14(b). A uniform shadow around the circumference of the disc indicates the disc is normal to the camera and therefore untilted. The source of this wobble is believed to be an imbalance of forces created by the fluid exiting the manifold to one side. This behaviour has a couple of notable effects on the results. First, when the disc is wobbling, the edge of the disc bounces off the stop preventing the disc from fully opening. Second, when the pressure differential across the disc becomes negative and the valve begins the close, if the disc is tilted or bouncing off the stop, its centre of mass is nearer to the seat, causing it to close faster than a fully open valve. These effects are observed in Figures 10–13.

Another feature of the measurements is the varying seating distance. This is especially apparent in Figure 11–13. The disc is not constrained from rotation and therefore does not necessarily seat normal to the x-axis.

Figure 9. Inlet valve actual scale factor.
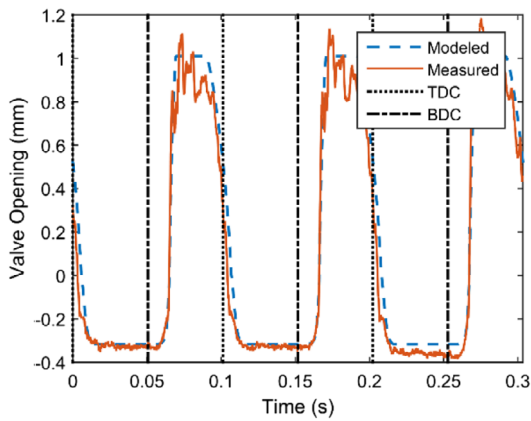
Figure 11. Delivery valve position, baseline.
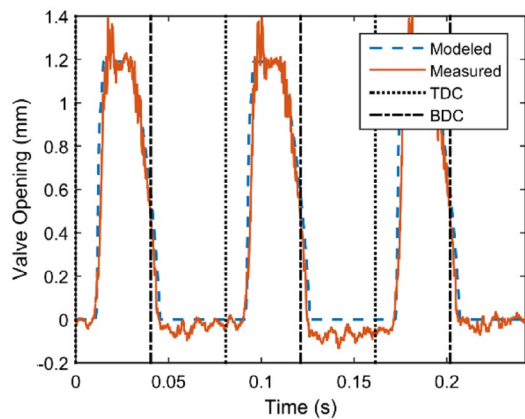
Figure 12. Inlet valve position, high speed.
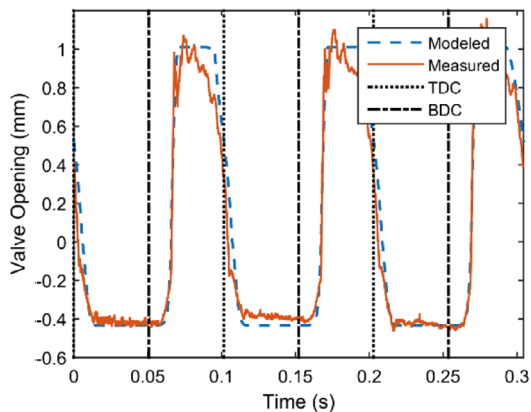
Figure 13. Delivery valve position, high pressure.

This can lead to slight variations in the measured position of the seated disc.

Inclination of the disc may lead to some error in the measured position. If this were the case, wobbling of the disc would result in an oscillatory position measurement. High speed camera footage also shows the disc bouncing in the x-direction. Therefore, the effect of each phenomena cannot be captured independently. Additionally, small air bubbles can be seen in the oil. This changes the effective refractive index of the oil, further contributing
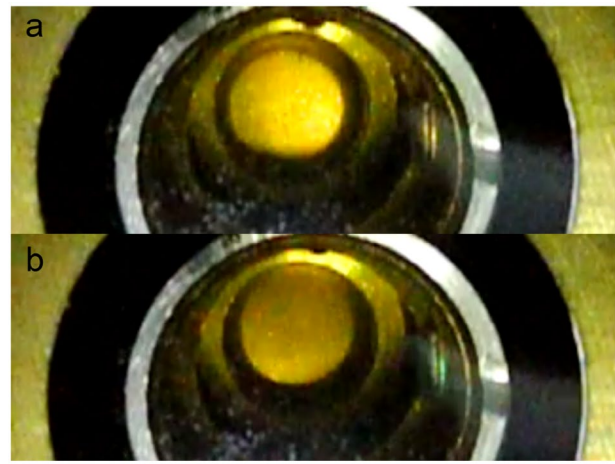
Figure 14. Untilted disc (a) and tilted disc (b).

to noise in the measurements. Despite these disturbances, the oscillations in the position measurements are on the order of 0.1 mm. While measurements were not taken using the high speed camera, qualitatively, the magnitude of oscillations in the actual disc appear to be on the order of the measured oscillations. It should be noted that no cavitation was observed or measured.

As a result of the delay in valve closing, backflow occurs, reducing the average flow rate of the pump. Since valve timing has a significant effect on the amount of backflow, the predicted flow rate is an important metric for evaluating the performance of a check valve model. Figure 15 shows the modelled flow rate through the inlet and delivery valve. The regions of negative flow rate indicate back flow through the check valves.

The pump delivery per revolution is the volume of fluid pumped per revolution, which is calculated by integrating the delivery valve flow rate over one revolution. In the experimental setup, the gear flow metre downstream of the VO measures the average flow rate of the pump. The pump delivery is then calculated by dividing the average flow rate by the pump speed. Table 6 compares the displaced volume of the pump with the modelled and experimentally measured pump delivery per revolution. The error between the modelled and measured pump delivery for the high speed case is an order of magnitude larger than the other cases. The modelled and measured pump delivery for each case falls within the range of 1.71–1.73 cc/rev with the exception of the measured delivery in the high speed case. Since the high speed case is not significantly faster than the other cases, it is unlikely that there is a marked drop in the pump delivery at 750 rpm. One possible explanation is the that pump had not reached steady state operation and the accumulator was still charging causing the measured flow rate to be lower than the flow rate out of the delivery valve.

Three assumptions made during construction of the pump and valve model will now be discussed. The first is that leakage is negligible. Due to the extremely tight clearance achieved between the piston and cylinder
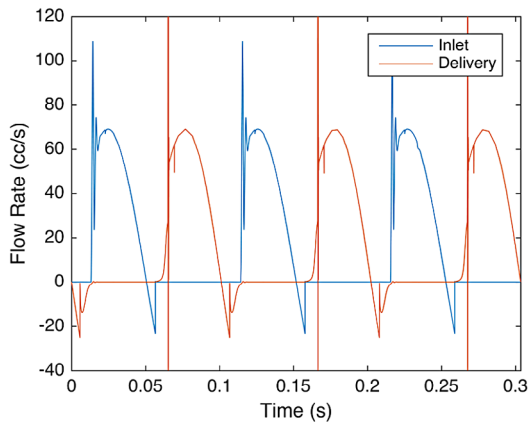
Figure 15. Modelled flow rate, baseline.

Table 6. Pump displacement.

	Baseline	High pressure	High speed
Displaced volume	2.217 cc	2.217 cc	2.217 cc
Modelled delivery	1.722 cc/rev	1.715 cc/rev	1.727 cc/rev
Measured delivery	1.720 cc/rev	1.713 cc/rev	1.684 cc/rev
Error (%)	0.1162	0.1170	2.521
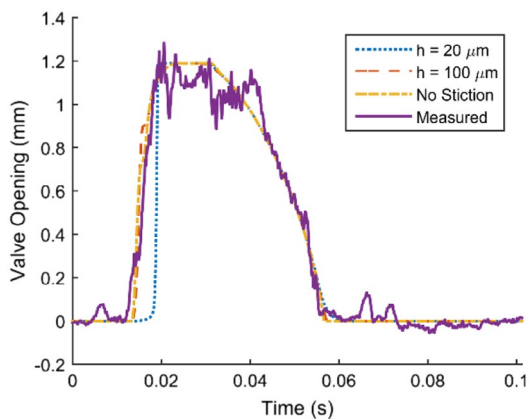
Figure 16. Effect of stiction on inlet valve opening, baseline.

and relatively low operating pressure, no leakage was observed during experiments. Second is that stiction forces are negligible. Estimating the minimum oil gap thickness in Equation (16) is difficult, so a range of values were modelled and compared to experimental results as shown in Figure 16, where h in the legend is the minimum gap thickness. Model results neglecting stiction forces agree more closely with experimental results than those including stiction. Based on these results, two explanations are proposed. The first is that due to valve geometry or seating, the minimum gap thickness is large enough that the stiction force is negligible. The effect of stiction force rapidly decreases with minimum gap thickness due to the inverse third power relationship in Equation (16). The second explanation is that since the disc is not constrained to remain parallel to the seat, it is opening at an angle, rendering Equation (16) invalid and reducing the stiction force

to a negligible level. Whether one or both of the effects are occurring, the result is that, for the experiments performed, the assumption that stiction is negligible was confirmed.

The third assumption is that both steady and transient flow forces are negligible. Both the flow rate and its time derivative are greatest during delivery valve opening as shown in Figure 15. Assuming flow rate and fluid acceleration are dominated by disc motion during opening, the maximum instantaneous steady and transient flow forces calculated from the valve position measurement are 0.2 and 2.2 N respectively, compared to the pressure force which exceeds 85 N. Based on these results, it is reasonable to neglect flow forces for the operating conditions explored.

6. Conclusion

In this paper, a hydraulic check valve model has been presented in the context of a piston pump. Pressure, spring, contact, stiction, and flow forces were calculated. Across the range of experimental conditions investigated, stiction and flow forces were found to be negligible. Flow through the valve was modelled using the steady orifice equation with an empirical discharge coefficient correlation. The discharge coefficient was found to be a strong function of the Reynolds number, with a value significantly less than the constant value of 0.6 commonly assumed when modelling orifices.

A method of accurately measuring valve position at high frequencies using laser triangulation was developed. The approach includes methods to characterise the refractive index of materials and calculate a correction scale factor for distance measurements through multiple materials. By doing so, the LTS is no longer limited to use in air and can be used to measure position change through multiple transparent interfaces.

The check valve model proposed in this paper accurately predicted the timing of valve opening and closing as well as position during transition events across a range of operating conditions. Wobbling of the disc was observed in experiments in contrast to the model which constrains the disc to one degree of freedom. This effect causes the modelled valve motion to deviate slightly from the measured behaviour while the valve is fully open. Despite this limitation, the overall valve dynamics were captured well by the model allowing the average flow rate to be predicted within 3% for all cases.

In future work, the model can be expanded to predict the disc wobble and its effects on valve response and flow rate. A more accurate method for calculating flow forces, such as utilizing computational fluid dynamics, would improve estimates of the flow forces to determine their relative significance and effect on valve dynamics. Furthermore, implementing a predictive rather than experimental method of calculating the discharge coefficient correlation would aid in valve optimisation.

Validation over a wider range of operating conditions, valve architectures, and circuit types would increase confidence in the model.

Disclosure statement

No potential conflict of interest was reported by the authors.

Funding

Notes on contributors

Anthony L. Knutson is a PhD student at the University of Minnesota in the Department of Mechanical Engineering. He conducts research in the Mechanical Energy and Power Systems Laboratory, which he first joined as an undergraduate in 2013. Anthony's research interests are broad and include hydraulic circuit modelling and experimental design, medical device design, and computational fluid dynamics.

James D. Van de Ven is an assistant professor and McKnight Land-Grant professor at the University of Minnesota in the Department of Mechanical Engineering where he operates the Mechanical Energy and Power Systems (MEPS) Laboratory. Professor Van de Ven received his PhD in Mechanical Engineering from the University of Minnesota in 2006. From 2007 to 2011, he was an assistant professor in the Mechanical Engineering Department at Worcester Polytechnic Institute. Prior to joining WPI, Dr Van de Ven was a Post-Doctoral Research Associate at the University of Minnesota in the NSF sponsored Engineering Research Center for Compact and Efficient Fluid Power. Dr Van de Ven's research interests are in efficient energy conversion, energy storage, fluid power, kinematics, and machine design.

ORCID

Anthony L. Knutson http://orcid.org/0000-0002-1391-3576

References

Budwig, R., 1994. Refractive index matching methods for liquid flow investigations. *Experiments in fluids*, 17 (5), 350–355.

Cho, B.H., Lee, H.W. and Oh, J.S., 2002. Estimation technique of air content in automatic transmission fluid by measuring effective bulk modulus. *International journal of automotive technology*, 3 (2), 57–61.

Chu, K.Y. and Thompson, A.R., 1962. Densities and refractive indices of alcohol–water solutions of n-propyl, isopropyl, and methyl alcohols. *Journal of chemical and engineering data*, 7 (3), 358–360.

Edge, K.A., Brett, P.N. and Leahy, J.C., 1984. Digital computer simulation as an aid in improving the performance of positive displacement pumps with self-acting valves. *ARCHIVE: Proceedings of the institution of mechanical engineers, Part B: Management and engineering manufacture 1983–1988 (vols 197–202)*, 198 (14), 267–274.

Hamrock, B.J., Schmid, S.R. and Jacobson, B.O., 2004. *Fundamentals of fluid film lubrication*. New York, NY: CRC Press.

Johnston, D.N., 1991. Numerical modelling of reciprocating pumps with self-acting valves. *Proceedings of the institution of mechanical engineers, Part I: Journal of systems and control engineering*, 205 (2), 87–96.

Lee, J.K., Jung, J.K., Chai, J.B. and Lee, J.W., 2015. Mathematical modeling of reciprocating pump. *Journal of mechanical science and technology*, 29 (8), 3141–3151.

Merritt, H.E., 1967. *Hydraulic control systems*. New York, NY: Wiley.

Peterson, J.P. and Peterson, R.B., 2006. Laser triangulation for liquid film thickness measurements through multiple interfaces. *Applied optics*, 45 (20), 4916–4926.

Wu, D., Burton, R. and Schoenau, G., 2002. An empirical discharge coefficient model for orifice flow. *International journal of fluid power*, 3 (3), 13–19.

Yudell, A.C. and Van de Ven, J.D., 2015. Predicting solenoid valve spool displacement through current analysis. *International journal of fluid power*, 16 (3), 1–8.